Int. J. Electrochem. Sci., 12 **(2017)** 2112 – 2124, doi: 10.20964/2017.03.53

International Journal of
ELECTROCHEMICAL
SCIENCE
www.electrochemsci.org

Influence of Wavelength on Photo-Assisting Anodic Electrodeposition of Ceria Thin Films

Yang Yang [1], *Ze-gang Dong*[1], *Zhao Zhang* [2,*], *Yu Chen*[2], *Yin-ye Yang*[1], *Hai-jun Du*[3]

[1] School of Materials Science and Engineering, Guizhou Minzu University, Guiyang 550025, P. R. China
[2] Department of Chemistry, Zhejiang University, Hangzhou 310027, P. R. China
[3] School of Chemistry and Eco-Environmental Science, Guizhou Minzu University, Guiyang 550025, P. R. China
[*]E-mail: eaglezzy@zjuem.zju.edu.cn

Received: 31 July 2016 / *Accepted:* 19 January 2017 / *Published:* 12 February 2017

Cerium oxide films have been anodically deposited with photo-assisting onto 316L stainless steel in bath solution containing 0.05 M cerium (*III*) nitrate, 0.1 M ammonia acetate and 70 % (V/V) ethanol. Three monochromatic photo wavelengths (254 nm, 365 nm and 415 nm) have been discussed. The electroplating behaviors and the structural of the films were investigated with *i-t* curves, ellipsometry, scanning electron microscopy, glancing angle X-ray diffraction, and Raman and X-ray photoelectron spectroscopy. Results show that, photo irradiation favors the anodic growth of ceria films. With shortening the incident photo wavelength from 415 nm to 254 nm, the film thickness increase from 20.8 nm to 32.4 nm and the film crystallinity was enhanced. Moreover, shortening of the photo wavelength has a negligible effect on both the stoichiometry and the preferential occcbrientation growth of the deposits.

Keywords: Anodic electrodeposition; Photo irradiation; Ceria thin films

1. INTRODUCTION

Ceria (cerium oxide, CeO_2) has been applied in various areas, such as solid oxide fuel cells [1], polishing agents [2], catalysts of exhaust automobiles gas [3], electrochromic [4], and coatings for corrosion protection of metallic materials [5-11].

It is widely accepted that anodic electrodeposition is the most appropriate method to produce pure ceria films for that Ce^{3+} can be directly oxidized to soluble $Ce(OH)_2^{2+}$, and then the supersaturated $Ce(OH)_2^{2+}$ at the anode surface is deposited as solid CeO_2 [12, 13].

$$Ce^{3+} + 2H_2O \rightarrow Ce(OH)_2^{2+} + 2H^+ + e \quad (1)$$

$$Ce(OH)_2^{2+} \rightarrow CeO_2 + 2H^+ \quad (2)$$

However, anodic growth will be retarded once the electrode is covered with a layer of CeO_2 film due to its poor conductivity [12, 14]. Fortunately, CeO_2 as a kind of semiconductors which can absorb a certain wavelength of light, and cause the indirect transition of electrons from the valence band (O2p) to the empty Ce4f states, hence, favors their further electrochemical growth [15, 16]. The photo assisting electrodeposition of CeO_2 thin film can be described as following reactions [16-19],

$$CeO_2 + h\nu \rightarrow e_{cb}^- \cdots h_{vb}^+ \quad (3)$$

$$H_2O \xrightarrow{h\nu} \cdot OH + \cdot H \quad (4)$$

$$Ce^{3+} + h_{vb}^+ + H_2O \rightarrow Ce(OH)_2^{2+} + 2H^+ \quad (5)$$

$$Ce^{3+} + \cdot OH + H_2O \rightarrow Ce(OH)_2^{2+} + H^+ \quad (6)$$

$$Ce(OH)_2^{2+} + 2H_2O \rightarrow Ce(OH)_4 + 2H^+ \quad (7)$$

$$Ce(OH)_2^{2+} + 2OH^- \rightarrow CeO_2 + 2H_2O \quad (8)$$

$$Ce(OH)_4 \rightarrow CeO_2 + 2H_2O \quad (9)$$

The utilization of photon energy has been demonstrated to be of numerous advantages [20], such as the precise control of semiconductor nanoparticles size [21, 22] and the local electrochemical reactions by site-selective photon irradiation [23]. However, the influence of photon energy on deposition of ceria films has not been elucidated clearly. Therefore, the aim of the present work is to systematically study the effects of photo energy on the anodic electrodeposition of ceria films.

2. EXPERIMENTAL DETAILS

The electroplating bath consists of 0.05 M $Ce(NO_3)_3 \cdot 6H_2O$ (Analytical reagent (AR)), 0.1 M CH_3COONH_4 (AR) as a complex agent, 70 % (V) CH_3CH_2OH (AR) and double-distilled water. The bath solution pH is around 6.20.

Electrodeposition was conducted in a two-compartment cell. A commercial 316L stainless steel rod (SS, working area: 0.50 cm^2) was adopted as working electrode and which surface was polished to mirror before each experiment. The treated steel was dried with nitrogen gas (N_2) and then dipped into the anodic compartment for use. A large platinum foil (25 × 25 × 0.2 mm) was used as counter electrode (cathodic compartment). A saturated calomel electrode (SCE) was employed as reference, and all potentials in this paper were referred to SCE unless otherwise stated.

Electrodeposition was performed at a constant potential of 0.8 V and at solution temperature of 50 ± 0.1 °C for 40 min [24]. During the deposition, the working electrode surface was exposed to different lights. The light source was a 500 W Xe lamp, whose intensity is around 108 $mW \cdot cm^{-2}$ (measured using novall ophir laser measurement group). The adopted monochromatic lights of 254, 365 and 415 nm were achieved using a monochromator, whose irradiances are about 13.2, 3.7 and 4.6 $mW \cdot cm^{-2}$, respectively. After deposition, all samples were cleaned with double-distilled water and dried by N_2 gas, and then stored in a desiccator for further examination.

Thickness and refractive index of the films were determined by ellipsometry which was collected at three angles from the surface plane (65°, 70° and 75°) with an M-2000 series ellipsometer (J. A. Woollam). The porosity of the films has been estimated using Lorentz–Lorentz formula (Eq. 10) which is related to the measured refractive index [25, 26].

$$Porosity = 1 - \left(\frac{n^2 - 1}{n^2 + 2}\right)\left(\frac{n_0^2 + 2}{n_0^2 - 1}\right) \qquad (10)$$

where n is the measured refractive index of the film and n_0 is the bulk refractive index (n_0 = 2.34).

Surface morphologies were observed by scanning electron microscope (SEM, Hitachi SU70). The structure and composition were identified by glancing angle X-ray diffraction (XRD), Raman and X-ray photoelectron spectroscopy (XPS). The XRD patterns were conducted with a RIGAKU D/MAX 2550 diffractometer using Cu Kα radiation (λ = 0.154056 nm) at a scan rate of 5 °/ min, and the tube source was operated at 40 kV and 250 mA. The Raman spectra were recorded with a LabRam HRUV spectrometer, equipped with a confocal microscope with a focal spot size about 40 micrometers, using an incident beam of 514 nm emitted by an argon laser. The XPS were performed on a VG ESCALAB MARK II spectrometer with Mg Kα radiation (1253.6 eV), operating at constant pass energy mode at 50 eV. The surface charging effect was corrected by fixing the *C1s* peak at a binding energy of 284.6 eV.

3. RESULTS AND DISCUSSION

The thickness, refractive index and porosity of the films are listed in Table 1. It shows that the film porosity gradually increases with the irradiation wavelength varying from 254 nm to 415 nm, while, the film thickness decreases from 32.4 nm to 20.8 nm, and all these film thicknesses are larger than that obtained under the same deposition conditions without photo illumination (17.1 nm) [27].

Table 1. The thickness, refractive and porosity of the deposited films

Wavelength / nm	254	365	415
Thickness (δ) / nm	32.4	30.5	20.8
Refractive index	1.88	1.86	1.74
Porosity / %	23.51	24.75	32.64

Kamada et al [20] reported that UV irradiation favors continuous growth of CeO_2 film, since the band gap excitation of the pre-formed CeO_2 particles under the irradiation, and producing electrons (e_{cb}^-) and holes (h_{vb}^+) in their conduction and valence bands, respectively. Then, Ce^{3+} ions adsorbed on the electrode surface can be oxidized by the h_{vb}^+ to form new CeO_2 nuclei on the preformed ceria films.

In addition, OH radicals which produced by the reaction between holes and water molecules may also benefit the Oxidation [20].

According to formula (11), it is known that CeO_2, whose band gap is known to be 3.1 *eV*, can only absorb the light wavelength shorter than 400 nm by indirect transition of electrons from the valence band (O*2p*) to the empty Ce*4f* states [19]. Photons of energy greater than the band gap of CeO_2 produce electron-hole pairs, and the photo-generated holes are driven to the surface by the electric field in the depletion region [28].

$$\lambda_g(nm) = \frac{1240}{E_g(eV)} \qquad (11)$$

where λ_g is the maximum excited wavelength, E_g is band gap energy of semiconductor. Therefore, the effective photo irradiation wavelengths in this study are 365 nm and 254 nm. Moreover, it seems that the wavelength of 415 nm is not enough for the excitation of electrons from the conduction band to the valence band, but the light has a high enough energy to generate electron-hole pairs inside the semi-conductor [28], and it can at least enhance the conductivity of CeO_2 film. Hence, the film thickness for 415 nm is higher than that without photo illumination [27].

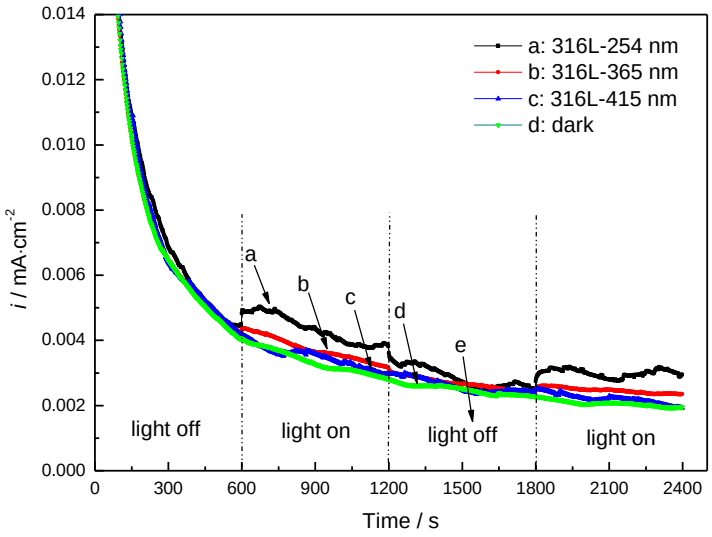

Figure 1. The *i-t* curves of the 316L electrode in the bath solution with intermittently lights off and on at an interval of 10 min under different photo wavelengths

The beneficial action of photo irradiation on the anodic growth of ceria films can also be demonstrated by the relationship between the deposition current density (*i*) and the deposition time (*t*) (Fig.1), which are obtained during the depositing processes of ceria films with the intermittent photo irradiation (at an interval of 10 min). In the initial 10 min without photo illumination, all current densities decrease quickly and monotonously due to the poor conductivity of the preformed ceria film, all current densities with photo irradiation are larger than that of no photo illumination (dark). Fig.1 also interestingly shows that *i* can be ordered in the following sequence: 254 nm ≥ 365 nm ≥ 415 nm ≥ dark, which clearly suggests that the growth rate of ceria films is closely related to the used photo energy. The average current densities of two light-on parts for 254 nm, 365 nm and 415 nm photo

irradiation are 3.67×10^{-3} mA·cm^{-2}, 3.10×10^{-3} mA·cm^{-2} and 2.86×10^{-3} mA·cm^{-2} , respectively, all of those are somewhat larger than that of the same parts of no photo irradiation (2.72×10^{-3} mA·cm^{-2}). Therefore, the film thickness decreases with increasing the wavelength of photo irradiation (Table 1). If presumably designate the total contribution of both the applied anodic potential and the natural light in our lab (dark condition) to the average depositing current density (i) is one unit, then the relative contribution of the used photo irradiation to i (designated as RC) can be calculated as 34.93 %, 13.97 % and 5.15 % for the photo of 254 nm, 365 nm and 415 nm, respectively. It shows that the larger the RC value, the thicker the CeO_2 film (Table 1).

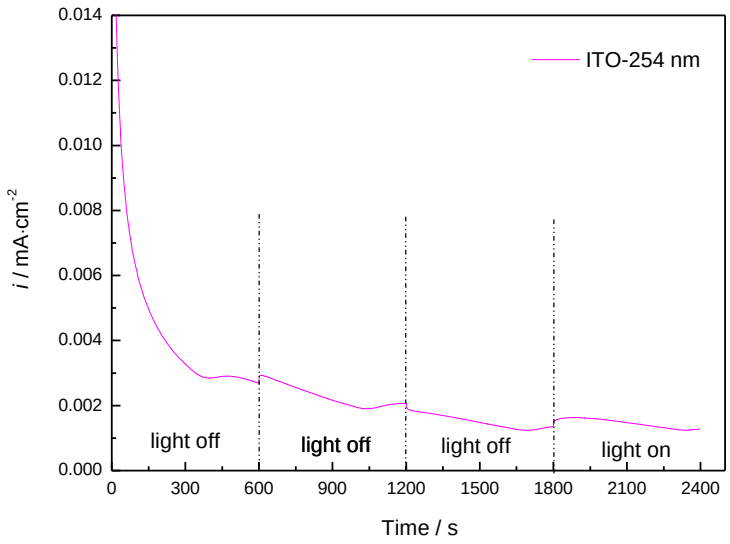

Figure 2. The *i-t* curves of ITO electrode in the bath solution with intermittently light off and on at an interval of 10 min

In addition, whether the photo currents are come from the passive film on the 316L electrode or the as-deposited ceria thin film? The ITO electrode and 254 nm photo irradiation were used (Fig.2). It can be seen that with light on, the photo current has increased as the same trend with 316L electrode, which suggests that the photo current is come from the absorption of as-deposited ceria thin film and the photo irradiation favors the deposition of ceria thin film.

However, when compare the calculated RC value with that of the films thicknesses (Table 1), it is found that the film thickness of 254 nm photo irradiation is only 1.90 nm larger than that of 365 nm. The reason may be that the electroplating solution mainly absorb the light shorter than 350 nm, and the absorptivity increases with the decrease of photo irradiation wavelength (Fig.3).

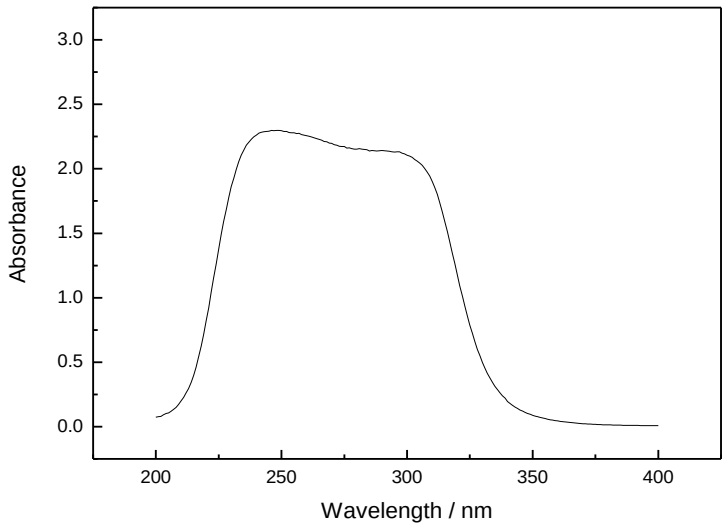

Figure 3. The UV-absorbance spectrum of the deposition bath solution

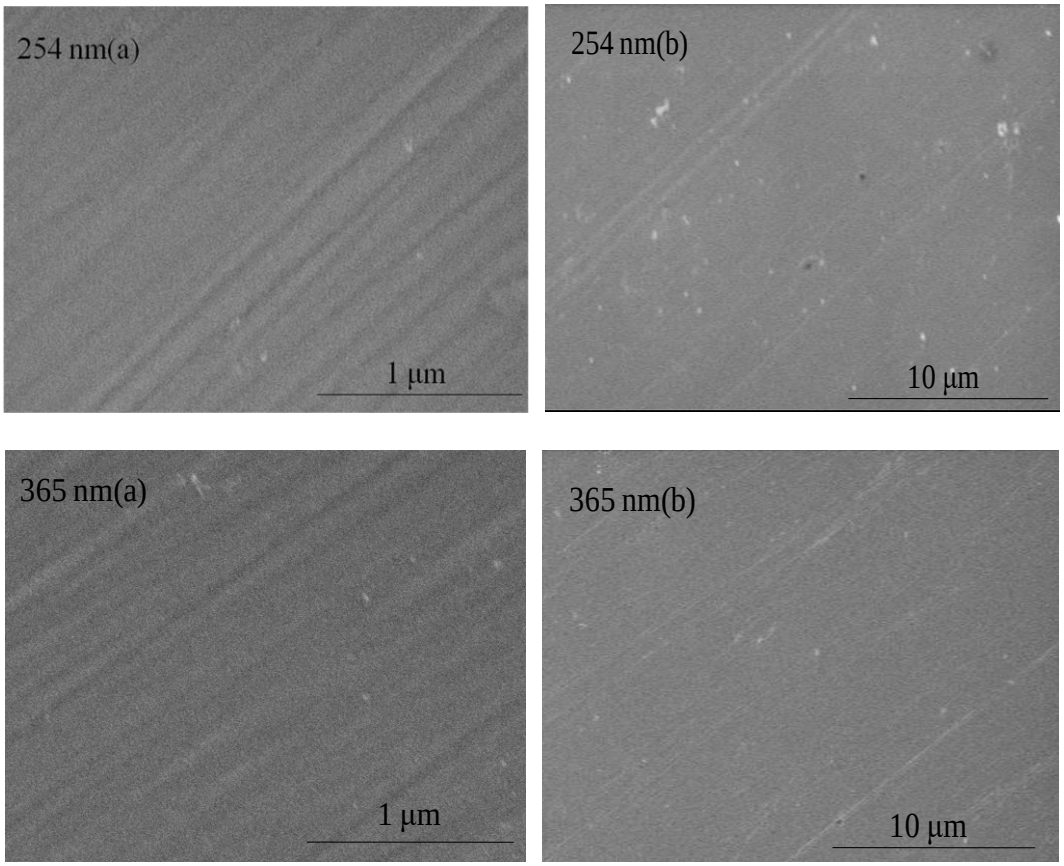

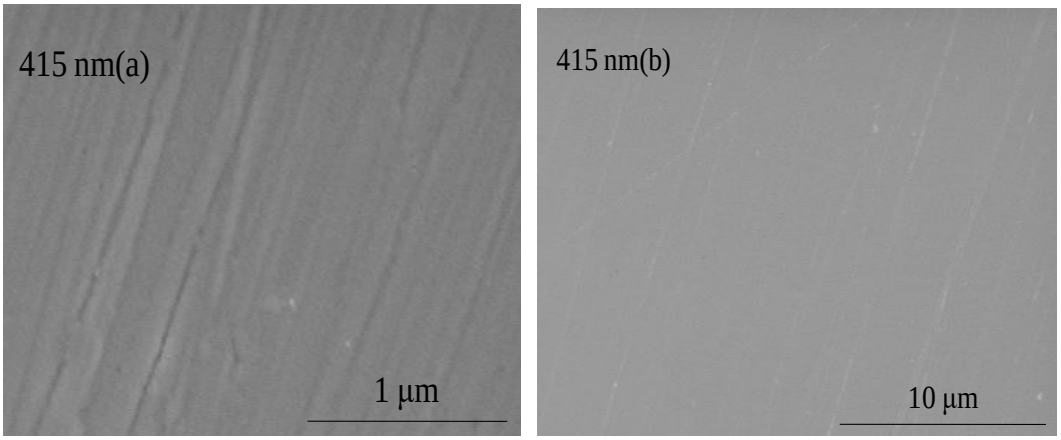

Figure 4. SEM surface morphology of the deposits (a) and the corresponding enlarged image (b).

Surface morphologies of the deposited ceria films were observed by SEM. It can be clearly seen that all films are smooth and compact (Fig. 4). The obvious polishing scratches can be observed on 316L substrates (Fig. 4a), which can be attributed to the ultrathin thickness of the obtained ceria films (Table 1). In the case of 254 nm, larger electroplating current density (Fig. 1) results in the formation of some particles (cerium oxide or hydrated oxide) on the substrate surface. These particles number decrease with increasing the wavelength of photo irradiation (Fig. 4b), and such particles can hardly be observed on the films obtained without light illumination [27]. The origination of such white particles can at least be attributed to the local oxidation of the intermediate products (such as $Ce(OH)_3$ and Ce_2O_3) on the substrate by the dissolved oxygen in bath solution [27], the co-deposition of the hydrolysis products [29] of Ce^{3+} ions in solutions, and the entrapped (hydrated) CeO_2 nanoparticles formed also in solutions by the photo-generated nitrite ions that act as a kind of photo-oxidizing agents [19]. However, the only change in all electroplating tests of this study is the photo wavelength, which should be certainly responsible for the difference of the particle numbers. Moreover, the UV-absorbance spectrum (Fig.3) can also suggest these particles are formed by photo-oxidation of the bath solution.

Fig. 5 shows the glancing angle XRD patterns of the deposited films. All of the XRD patterns clearly show the existence of (111) and (220) crystallographic planes of CeO_2 (PDF No. 34-0394). The intensity of (220) is the highest for all samples, which agrees well with the anodic deposition results without light illumination in our previous studies [24, 27]. Therefore, photo irradiation does not change the crystal orientation of the deposits. Moreover, the intensity of (220) increases with shortening photo wavelength, suggesting the crystallinity of the film was enhanced by the light with shorter wavelength. In addition, the reflection of Ce_2O_3 has been observed which should be related with the photo oxidization of Ce^{3+} or following reaction [29],

$$2Ce^{3+} + H_2O \rightarrow Ce_2O_3 + 6H^+ \qquad (12)$$

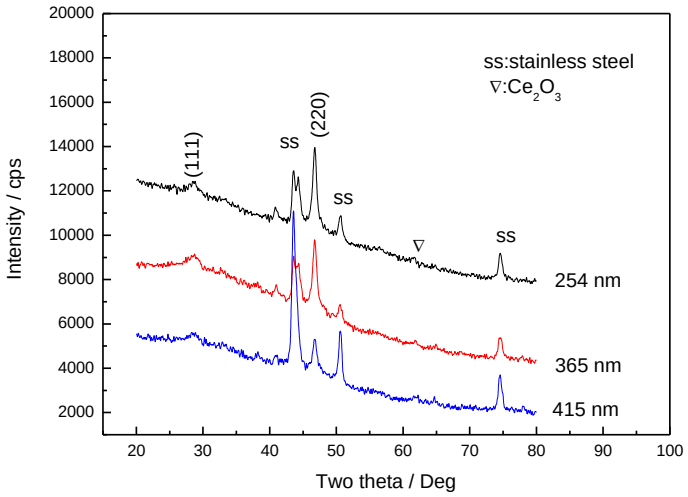

Figure 5. XRD patterns for the deposited cerium oxides films.

Raman spectroscopy was employed to evaluate the film structure and crystallinity (Fig. 6). It can be seen that all spectra present an intense band at 454 cm^{-1}, which has been attributed to the F2g mode of the fluorite structure of CeO_2 [30, 31]. This peak is broaden and red-shifted as compared to the bulk CeO_2 (464 cm^{-1}), and seems to be strongly influenced by the particle size and the oxygen vancancies in the deposits [30, 31]. The intensity of this band increases with decreasing the wavelength, which may be related to the film thickness and the enhanced crystallization [12].

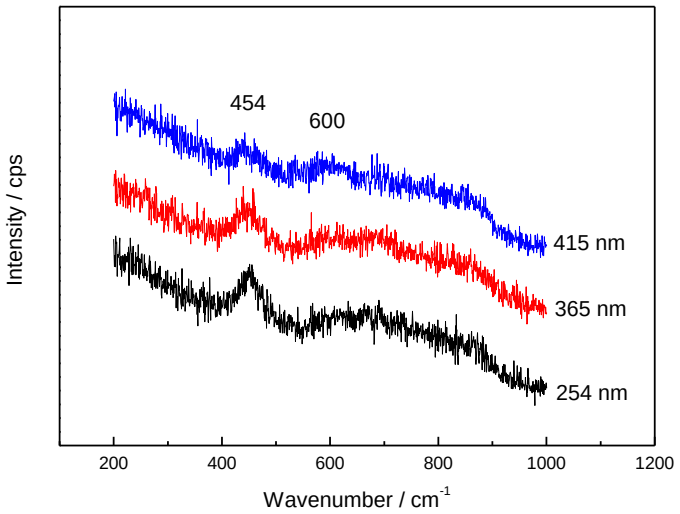

Figure 6. Raman spectra for the deposited cerium oxides films.

XPS was used to analyze the chemical composition of the deposited films. The typical *Ce3d* spectra are illustrated in Fig.7. There are eight peaks assignment in the spectra, which are labeled using the notation of Burroughs [32]. Peaks *U*, *U''*, *U'''* and *V*, *V''*, *V'''* refer to $3d_{3/2}$ and $3d_{5/2}$, respectively. The doublet *U/V* are attributed to the state of Ce(*IV*) $3d^9 4f^2 O2p^4$; doublet *U''/V''* correspond to the hydridization state of Ce(*IV*) $3d^9 4f^1 O2p^5$; and the doublet *U'''/V'''* are assigned to the final state of

Ce(*IV*) $3d^9 4f^0 O2p^6$, the best characteristic peak to differentiate Ce(*IV*) from Ce(*III*) is the binding energy at around 917 eV; While *U'* and *V'* are present for Ce(*III*) *3d* final states.

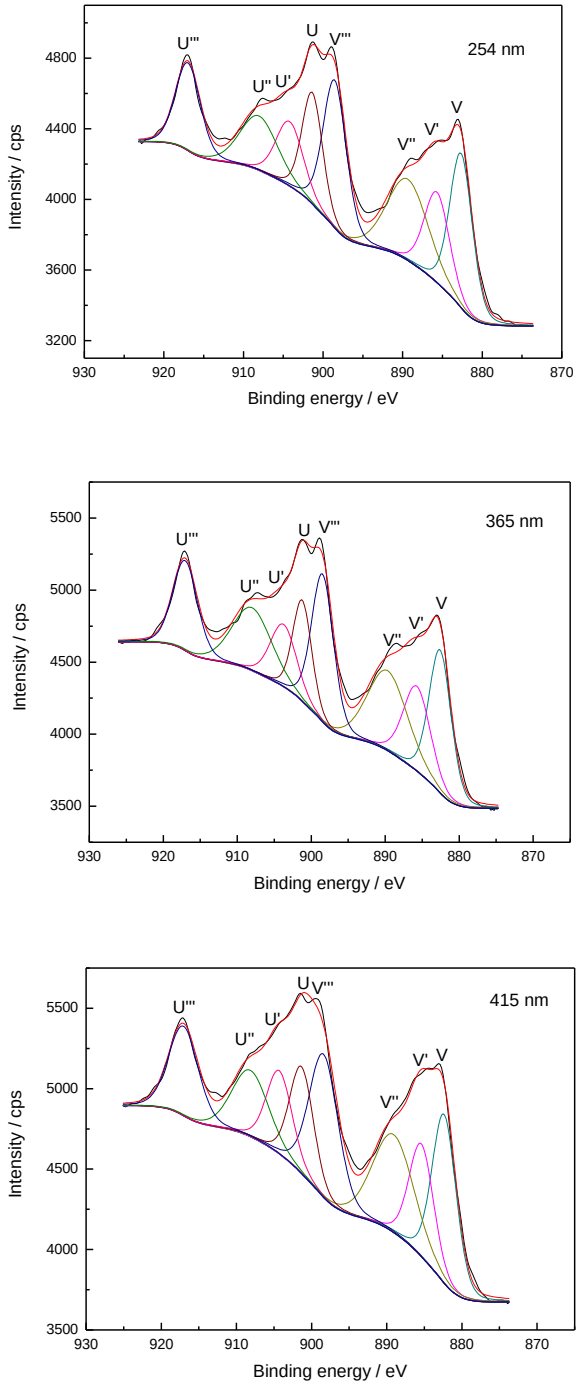

Figure 7. The *Ce3d* spectra for the deposited cerium oxides films.

The stoichiometry of cerium oxide was estimated by the method of Fallah (Eq. 13) [33], Using this method, the fitted peak areas in the *Ce3d* spectra can be used to estimate the contribution of Ce(*IV*) and Ce(*III*) for the deposited films.

$$Ce(III) = \frac{\left(U^0 + V^0 + U' + V'\right)}{\left(U^0 + V^0\right) + \left(\sum_{n'} \left(U^{n'} + V^{n'}\right)\right)} \qquad (13)$$

where the U^0, V^0 do not appear for the electrodeposited nanocrystalline films [34], *n'* is for all states. The calculated ratio between Ce(*IV*) and Ce(*III*) shows that, the deposited films are mostly in the state of Ce(*IV*) oxidation, and the calculated stoichiometry is around $CeO_{1.90}$ for all samples, which is in accordance with the dark conditions [27].

The non-stoichiometry of the obtained ceria films can also be proved by the present of the intense band at 600 cm^{-1} (Fig. 6), which corresponds to the asymmetry Ce-O peak belonging to the oxygen vacancies in cerium oxide films and has been attributed to the introduction of Ce(*III*) into CeO_2 lattice [34]. In addition, at different wavelength, the calculated amount of Ce(*IV*) for the ceria films is almost the same (ca. 80.59%, 80.49% and 80.24% for the wavelength of 254 nm, 365 nm and 415 nm respectively).

Fig. 8 shows the *O1s* spectra for the electrodeposited cerium oxide films. The *O1s* can be separated into three peaks by fitting the data with a Gaussian/Lorenzian lineshape and fixing the full-width at half-maximum of 2.2 eV for each peak, labeled as *A*, *B* and *C* [11, 35, 36]. Peak *A* (at around 529.7 eV) is attributed to O-Ce bonds from the structure of cerium oxide (CeO_2) [37].

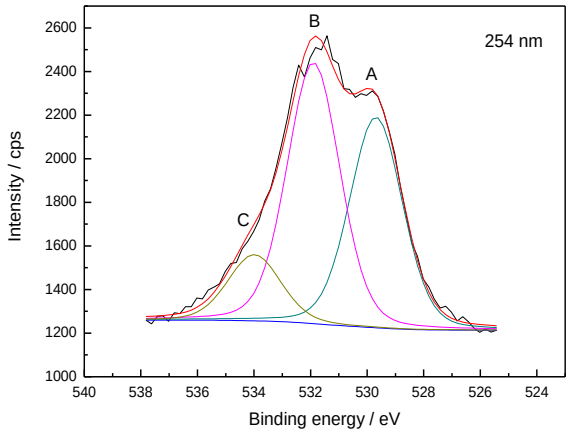

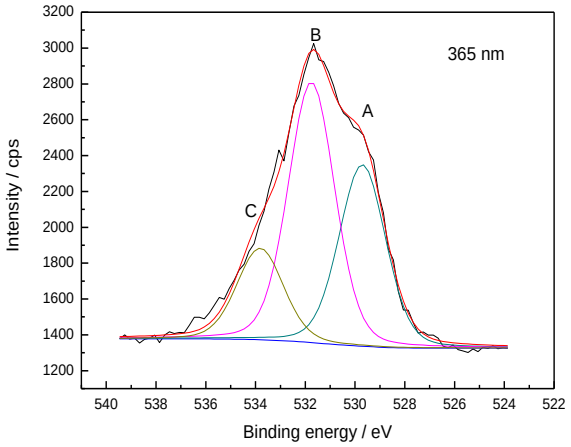

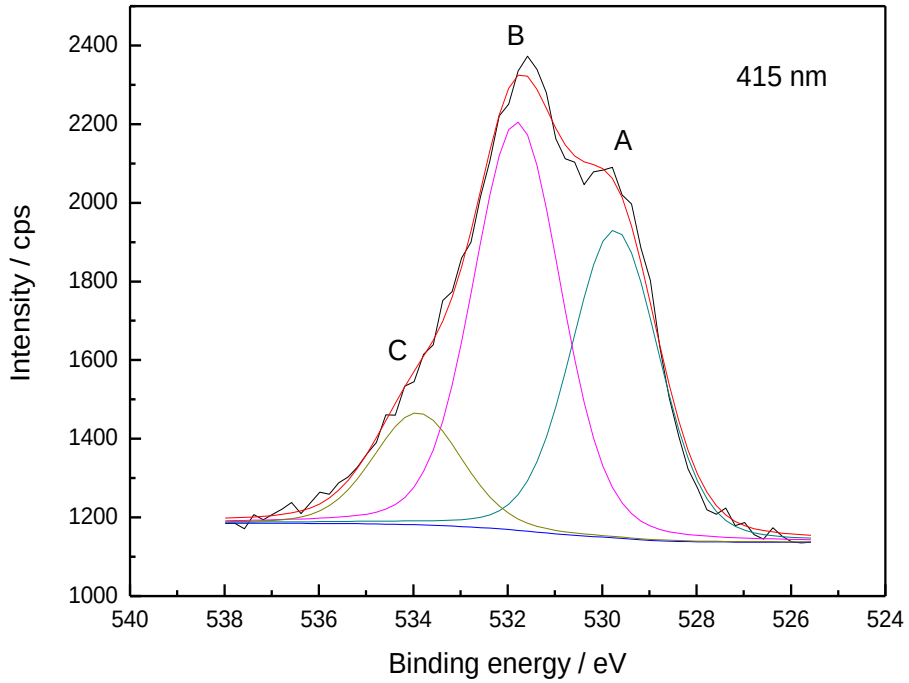

Figure 8. The *O1s* spectra for the deposited cerium oxides films.

Peak B appears at a binding energy around 531.8 eV due to hydroxidic species [11, 37], which demonstrates the existence of cerium hydroxyl compounds (like $Ce(OH)_4$). Peak *C* could be due to the absorbed H_2O and / or adsorbed oxygen on the electrode surface [11]. With the increase of irradiation wavelength from 254 through 365 to 415 nm, the area of peak A decreases from 40.95 % through 37.19 % to 34.03 %, while that of peak B simultaneously decreases from 50.75 % through 49.28% to 48.81 %.

From the above XPS results, it can be concluded that the decrease the irradiation wavelength has negligible effect on the content of Ce(*IV*) in ceria films, but slightly increases the amount sum of the cerium oxide (CeO_2) and hydroxyl compounds (like $Ce(OH)_4$).

4. CONCLUSIONS

All the cerium film thickness, compactness and crystallinity increase with shortening the investigated wavelengths (415 nm, 365 nm and 254 nm). The variation of photo irradiation wavelength does not change the preferential orientation and Ce(*IV*) content of the anodic deposited CeO_2 films, the stoichiometry is around $CeO_{1.90}$ for all samples, and the film obtained at wavelength of 254 nm contains the highest amount of cerium oxide (CeO_2) and hydroxyl compounds(like $Ce(OH)_4$), reaching 40.95 and 50.75 %, respectively.

ACKNOWLEDGEMENT
The authors wish to acknowledge the financial supports from the National Natural Science Foundation of China (Project 21073162, 51131005, 81260639, 21403194)), the Projects of Science and Technology Department of Guizhou Province (No. [2015]7220, [2016]1070), the Projects of Education Department of Guizhou Province (No. [2015]62, [2015]424, [2016]003), the Specialized Research Fund for the Doctoral Program of Higher Education (No. 20130101110047), the "Chun Hui" Cooperation Program of Ministry Education of China (No. Z2014086), the International Cooperation Program of Science and Technology of Guizhou Province (No. [2013]7042), and the Postdoctoral Science Foundation of China (Project 2016M601929).

References

1. E.P. Murray, T. Tsai, S.A. Barnett, *Nature*, 400 (1999) 649.
2. X.D. Feng, D.C. Sayle, Z.L. Wang, M.S. Paras, B.Santoral, A.C. Sutorik, T.T. Sayle, Y. Yang, Y. Ding, X.D. Wang, Y.S. Her, *Science*, 312 (2006) 1504.
3. R.D. Monte, J. Kašpar, *J. Mater. Chem*., 15 (2005) 633.
4. I. Porqueras, C. Person, E. Bertran, *Thin Solid Films*, 447-448 (2004) 119.
5. X.W. Yu, C.N. Cao, Z.M. Yao, D.R. Zhou, Z.D. Yin, *Corros. Sci*., 43 (2001) 1283-1294.
6. H.Y. Su, W.J. Li, C.S. Lin, *J. Electrochem. Soc*., 159 (2012) C219.
7. Y. Hamlaoui, C. Rémazeilles, M. Bordes, L. Tifouti, F. Pedraza, *Corros. Sci*., 52 (2010) 1020.
8. S.T. Aruna, C.N. Bindu, V. Ezhil Selvi, V.K. William Grips, K.S. Rajam, *Surf. Coat. Technol*., 200 (2006) 6871.
9. M.F. Montemor, M.G.S. Ferreira, *Electrochim. Acta*, 52 (2007) 6976.
10. M.F. Montemor, R. Pinto, M.G.S. Ferreira, *Electrochim. Acta*, 54 (2009) 5179.
11. X.Q. Huang, N. Li, H.Y. Wang, H.X. Sun, S.S. Sun, J. Zheng, *Thin Solid Films*, 516 (2008) 1037.
12. K. Kamada, K. Higashikawa, M. Inada, N. Enomoto, J. Hojo, *J. Phys. Chem*. C, 111 (2007) 14508.
13. T.D. Golden, A.Q. Wang, *J.Electrochem. Soc*., 150 (2003) C621.
14. A.Q. Wang, T.D. Golden, *J. Electrochem. Soc*., 150 (2003) C616.
15. R.G. Toro, G. Malandrino, I.L. Fragalà, R. Lo Nigro, M. Losurdo, G. Bruno, *J. Phys. Chem*. B, 108 (2004) 16357.
16. Y.M. Yang, X.Q. Du, Y. Yang, L.Jiang, Z. Zhang, J.Q. Zhang, *J. Electrochem. Soc*., 162 (2015) D166.
17. M. Fujii, K. Nagasuna, M. Fujishima, T. Akita, H. Tada, *J. Phys. Chem*. C, 113 (2009) 16711.
18. Y-t. Yu, P. Mulvaney, *Korean J. Chem. Eng*., 20(2003) 1176.
19. K. Kamada, K. Horiguchi, T. Hyodo, Y. Shimizu, *Cryst. Growth Des*., 11 (2011) 1202.
20. K. Kamada, A. Moriyasu, *J. Mater. Chem*., 21 (2011) 4301.
21. T. Torimoto, J.P. Reyes, K. Iwasaki, B. Pal, T. Shibayama, K. Sugawara, H. Takahashi, B. Ohtani, *J. Am. Chem. Soc*., 125 (2003) 316.
22. T. Torimoto, H. Kontani, Y. Shibutani, S. Kuwabata, T. Sakata, H. Mori, H.Yoneyama, *J. Phys. Chem.* B, 105 (2001) 6838.
23. R. Hayward, D. Saville, I. Aksay, *Nature*, 404(2000) 56.
24. Y. Yang, Y.M. Yang, X.Q. Du, Y. Chen, Z. Zhang, J.Q. Zhang, *Appl. Surf. Sci*., 305(2014) 330.
25. E.A. Kulp, S.J. Limmer, E.W. Bohannan, J.A. Switzer, *Solid state Ionics*, 178 (2007) 749.
26. M. Dutta, S. Mridha, D. Basak, *Appl. Surf. Sci*., 254 (2008) 2743.
27. Y. Yang, Y.M. Yang, T.W. Fu, J. Zhu, J.P. Fan, Z. Zhang, J.Q. Zhang, *Thin Solid Films*, 556 (2014) 128.
28. R.J. Phillips, M.J. Shane, J.A. Switzer, *J. Mater. Res*., 4 (1989) 923.
29. Y. Yang, Y.M. Yang, C.S. An, Z.N. Yang, X.Q. Du, Y. Chen, Z. Zhang, J.Q. Zhang, *J. Electrochem. Soc*., 161(2014) D644.

30. J. Creus, F. Brezault, C. Rebere, M. Gadouleau, *Surf. Coat. Technol*., 200 (2006) 4636.
31. Y. Hamlaoui, F. Pedraza, L. Tifouti, *Corros. Sci*., 50 (2008) 2182.
32. P. Burroughs, A. Hamnett, A.F. Orchard, G. Thornton, *J. Chem. Soc., Dalton Trans*., 17 (1976) 1686.
33. J.E. Fallah, L, Hilaire, M. Roméo, F. Le Normand, *J. Electron. Spectrosc. Relat. Phenom.,* 73 (1995) 89.
34. A.Q. Wang, P. Punchaipetch, R.M. Wallace, T.D. Golden, *J. Vac. Sci. Technol*., B, 21 (2003) 1169.
35. I.G. Casella, M. Gatta, *J. Electroanal. Chem*., 494 (2000) 12.
36. I.G. Casella, M. Contursi, *J. Electroanal. Chem*., 588(2006) 147.
37. E. Abi-aad, R. Bechara, J. Grimblot, A. Aboukais, *Chem. Mater*., 5(1993) 793.